Application of Sinusoidal Field Pole in a Permanent-Magnet Synchronous Machine to Improve the NVH Behavior Considering the MTPA and MTPV Operation Area

Aryanti Kusuma Putri, Sebastian Rick, David Franck, and Kay Hameyer, *Senior Member, IEEE*

***Abstract*—In this paper, various approaches to improve the noise, vibration, and harshness (NVH) behavior of a single-layer interior permanent-magnet synchronous machine (IPMSM) are evaluated. The studied machine is used in electric vehicles and has a maximum output power of 53.6 kW. The acoustic noise of the electrical machine is mainly generated due to vibration of the stator yoke, which is caused by the radial forces acting on the stator's teeth. The radial force is directly correlated with the flux density in the air gap. Through modification of the outer frame of the rotor, the composition of the air-gap field, which consists of the fundamental wave and its harmonics, can be modified. The distribution of the radial force density on the surface of the stator teeth will be affected and the dominant order of the radial force can be reduced selectively, which will improve its acoustic behavior.**

***Index Terms*—Acoustic and noise of electrical machines, air-gap flux, electric vehicles, force densities, permanent-magnet synchronous machine (PMSM), rotor pole shaping, sinusoidal field pole, torque harmonics.**

I. Introduction

THE role of electric vehicles in individual transportation has become significant in the recent years. Although electrical drives are known for the low noise emission when compared to combustion engine, significant acoustic problems originated from single tones attract particular attention. Combustion engines, in contrast to the electric motor, generate broadband noise. Noise from electric motor has a single tone characteristic and lies within the sensitive hearing range of humans, which is generally between 2 and 5 kHz [1]. The sound radiation is strongly dependent on the housing and the installation of the machine. The force excitations in an electrical machines vary with the machine's speed. If the main natural frequencies of the structure are excited, the intense vibration induces remarkable noise. For a feasible acoustic evaluation, these aspects have to be considered. Therefore, structural dynamic and acoustic simulations have to be performed [2]. However, in the case that the dominant frequencies of the acoustic radiation are known, it is sufficient to analyze the exciting forces for the improvement of the electrical drive.

The major sources of noise in electrical machines are the periodic radial and tangential force waves acting on stator and rotor, respectively. The radial forces acting on the stator lead to the deformation of the housing. The tangential forces acting on the rotor leads to torque and torque pulsation. Both result in unwanted vibration of the machine parts, e.g., shaft, gearing, and differential. In case of a high-speed electrical machine with high number of poles and stator's teeth, the torque pulsation can also lead to unwanted noise. Since the sum of the torque depends on the integration of tangential forces and the axial length, the pulsation can be reduced by skewing the stator or rotor. The sum of the radial force harmonics on the stator circumference in a time step is null. In this case, the force densities distribution have to be analyzed. The force densities are related to the flux density waves on the air gap. As example in an induction machine with a squirrel cage rotor, these harmonics can be reduced by choosing specific numbers of stator and rotor slots [3]. In a salient-pole synchronous machine, the flux density harmonics can be reduced by altering the pole shoe shape of the rotor [4]. In a flux switching motor, the flux distribution can be influenced through notching the rotor [5].

The objective of this paper is to introduce a systematic approach to minimize the flux density harmonics of the air gap to reduce the acoustic radiation. The focus of this work lies on the improvement of the electromagnetic circuit through forming the rotor's surface and thus the shape of the air gap [4], [6], [7]. The rotor surface alteration methods are compared among each others and combined to achieve enhanced results. The stator, housing, and other machine components are not altered, so the time-consuming structural dynamic and acoustic simulations can be avoided. The resulting torque harmonics (temporal), which represent the sum of tangential force waves (spatial), and radial force density waves (temporal and spatial) are analyzed. The velocity on the stator surface caused by the radial force density waves acting on the stator teeth is evaluated. The proposed method is applied in a nonskewed single-layer interior permanent-magnet synchronous machine

Manuscript received June 15, 2015; revised September 28, 2015; accepted November 14, 2015. Date of publication February 19, 2016; date of current version May 18, 2016. Paper 2015-EMC-0346.R1, presented at the 2015 IEEE International Electric Machines and Drives Conference, Coeur d'Alene, ID, USA, May 10–13, and approved for publication in the IEEE Transactions on Industry Applications by the Electric Machines Committee of the IEEE Industry Applications Society.

The authors are with the Institute of Electrical Machines, RWTH Aachen University, 52062 Aachen, Germany (e-mail: aryanti.putri@iem.rwth-aachen.de; sebastian.rick@iem.rwth-aachen.de; david.franck@iem.rwth-aachen.de; Kay.Hameyer@iem.RWTH-Aachen.DE).

Color versions of one or more of the figures in this paper are available online at http://ieeexplore.ieee.org.

Digital Object Identifier 10.1109/TIA.2016.2532289

TABLE I
SIMULATION AND MACHINE PARAMETERS OF THE IPMSM

Stator outer radius $r_{\mathrm{stator},o}$	90 mm
Stator inner radius $r_{\mathrm{stator},i}$	61 mm
Air gap length δ	0.7 mm
Axial length l_{Fe}	120 mm
Number of poles / slots $2p/N$	12 / 36
Magnet type	NdFeB
Winding type	Distributed (q = 1)
Battery voltage U_{dc}	300 V
Maximum current (peak value) I_{max}	300 A
Rated torque M_N	155 Nm at 3300 min^{-1}
Rated power P_N	53.6 kW

(IPMSM). The simulation and machine parameters are listed in Table I. The results are analyzed for the entire operating area, which is defined through maximal torque per ampere (MTPA) in base speed and maximal through per voltage (MTPV) in field-weakening operating points [8]. To validate the proposed approach, structural dynamic and acoustic simulations are performed. The results are presented in [9].

II. METHODOLOGY

A. Analysis of the Radial Force Density Waves

The radial force density waves acting on the stator teeth are the major reason of the vibration of the stator's teeth, which leads to the deformation of the stator yoke. These force density waves can be traced back to the harmonics of flux densities, which originate from the rotor or stator. Generally, the flux density harmonics are caused by permanent magnets, stator slots and winding, and other effects, such as saturation and eccentricity. The radial force density waves $\sigma_{\mathrm{rad}}(\alpha,t)$ can be calculated with the simplified equation [10]:

$$\begin{aligned}\sigma_{\mathrm{rad}}(\alpha,t) &= \frac{B_{\mathrm{rad}}(\alpha,t)^2}{2\,\mu_0} \\ &= \frac{B_1(\alpha,t)^2 + 2\,B_1(\alpha,t)\,B_2(\alpha,t) + B_2(\alpha,t)^2}{2\,\mu_0},\end{aligned} \tag{1}$$

where α and t describe the position in the air gap and point in time. μ_0, B_{rad}, and B_1 and B_2 are the magnetic constant, sum of radial flux density in the air gap, and radial flux density from stator and rotor, respectively. After [11], the force density waves described in (1) can be decomposed according to its source of flux density waves. The force densities with m-th spatial order $\sigma^{\nu\nu}_{\mathrm{rad},m}$ or $\sigma^{\mu\mu}_{\mathrm{rad},m}$, which occur due to the flux density harmonics of stator or rotor in combination with itselves, respectively, are described with the following equations:

$$\begin{aligned}\sigma^{\nu\nu}_{\mathrm{rad},m}(\alpha,t) &= \frac{B^{\nu}_{\mathrm{rad}}(\alpha,t)^2}{2\,\mu_0} \\ \sigma^{\mu\mu}_{\mathrm{rad},m}(\alpha,t) &= \frac{B^{\mu}_{\mathrm{rad}}(\alpha,t)^2}{2\,\mu_0}.\end{aligned} \tag{2}$$

The force densities with m-th spatial order $\sigma^{\nu\mu}_{\mathrm{rad},m}$, which occur due to the combination of the flux density harmonics of stator and rotor, are described with the following equation:

$$\sigma^{\nu\mu}_{\mathrm{rad},m}(\alpha,t) = \frac{2\,B^{\nu}_{\mathrm{rad}}(\alpha,t)\,B^{\mu}_{\mathrm{rad}}(\alpha,t)}{2\,\mu_0}, \tag{3}$$

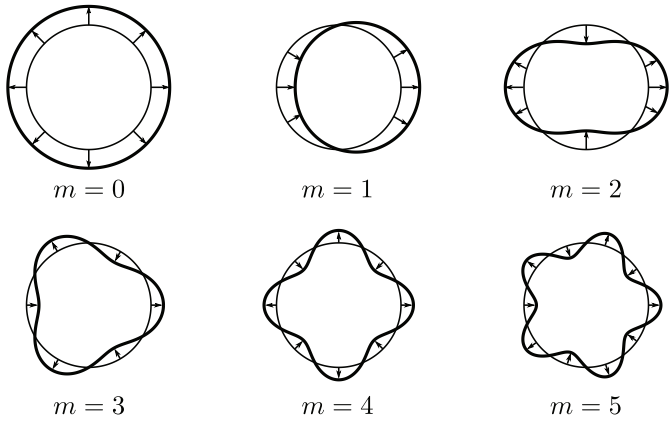

Fig. 1. Deformation of the stator yoke depending on spatial order m.

where B^{ν}_{rad} and B^{μ}_{rad} are the radial flux density ν-th order from stator and μ-th order from rotor (spatial), respectively. The deformation's amplitude m-th spatial order Y_m of the stator yoke, which is caused by these force densities, can be estimated with the following equations [3]:

$$\begin{aligned}Y_0 &= -\frac{r_{\mathrm{stator},i}\,N_{\mathrm{yoke}}}{E_{\mathrm{Fe}}\,h_{\mathrm{yoke}}}\sigma_{\mathrm{rad},0} \\ Y_1 &= \frac{4}{3}\frac{r_{\mathrm{stator},i}\,l_{\mathrm{Fe}}}{E_{\mathrm{Fe}}\,(\frac{d_{\mathrm{shaft}}}{L_{\mathrm{shaft}}})^4\,L_{\mathrm{shaft}}}\sigma_{\mathrm{rad},1} \\ Y_{m>=2} &= Y_0\left(\frac{2\sqrt{3}\,N_{\mathrm{yoke}}}{h_{\mathrm{yoke}}}\frac{1}{m^2-1}\right)^2\sigma_{\mathrm{rad},m},\end{aligned} \tag{4}$$

where d_{shaft} and L_{shaft} are the diameter of the shaft and the distance of the bearings, respectively. Assuming that the deformation of the stator is an oscillation in stationary state, the amplitude of surface velocities $\dot{Y}_m$ can be derived from the deformation amplitude Y_m:

$$\dot{Y}_m = 2\,\pi\,f_{\mathrm{mech}}\,s\,Y_m, \tag{5}$$

where f_{mech} and s are the mechanical rotation frequency and temporal order, respectively. The deformation of the stator yoke depending on spatial order m is illustrated in Fig. 1. A deformation with spatial order m rotates with the frequency $f_{\mathrm{mech}} * s$ and produces a tone with the same frequency. It is shown in (4) that the amplitude of the stator deformation Y_m decreases with $1/m^4$. Therefore, the relevant radial force densities, i.e., force density waves with low spatial order, correspond to the dominant amplitude of the stator deformation and thus its surface velocity. Hence, it is sufficient to analyze the amplitude of stator deformation or the surface velocity to determine the force densities, which are prominent to the acoustic radiation. The methods to calculate sound pressure level (SPL) from surface velocities with validated measurements are described in [12].

Through convolution of a radial force density wave, the time and spatial orders of the flux densities, which have major contribution to the radial force density, can be determined [13]. The terms in (1) can be two-dimensional (2-D) Fourier transformed and the equation can be rewritten in:

$$\sigma_{\mathrm{DFT2}}(s,m) = \frac{B_{\mathrm{DFT2}}(s,\nu/\mu) * B_{\mathrm{DFT2}}(s,\nu/\mu)}{2\,\mu_0}. \tag{6}$$

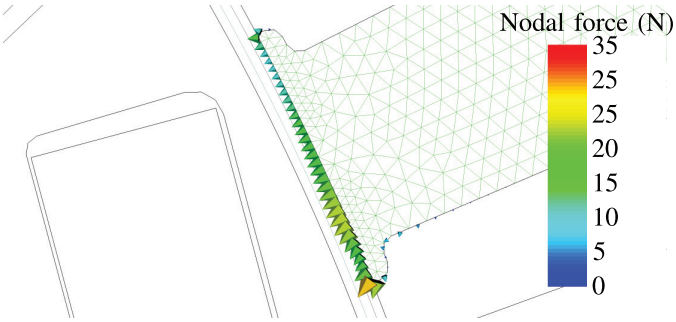

Fig. 2. Average of nodal forces between two neighboring nodes.

The Fourier transformed force and flux densities (σ_{DFT2} and B_{DFT2}, respectively) are dependent on temporal order s and spatial orders of the following:

1) force density waves m;
2) flux density waves originated from stator ν;
3) flux density waves originated from rotor μ.

To determine the origin of the flux density waves, finite-element (FE) simulations of rotor with magnetic ideal slotless stator or stator with magnetic ideal rotor ($\mu_r \to \infty$ or Neumann boundary condition) need to be performed. As a result, the source of flux density harmonics in the air gap can be separated.

B. Analysis of the Tangential Force Density Waves

According to [14] based on eggshell method [15], the sum of the forces F_k on every node k (nodal force) multiplied by its distance to the origin of the rotor r_k represent the torque T in one point in time. It is described with the following equation:

$$T = \Sigma\, r_k \times F_k. \tag{7}$$

Due to the cross product, only the tangential nodal forces have influence on the torque. Through implementation of (7) for multiple time steps up to one rotation of the rotor, the mean torque and torque harmonics can be calculated. Through analyzing the time-dependent torque, the effect of the tangential force densities wave can be studied.

C. Implementation

The first step of the approach is to perform FE simulations to determine the nodal forces on the air-gap side of the stator's surface. The force density waves acting on the stator are calculated through averaging two neighboring nodal forces (Fig. 2) and dividing its value by the distance between the two nodes and the axial length of the machine. The force densities should be decomposed in radial and tangential components. Through 2-D Fourier transformation, the force densities can be decomposed in temporal and spatial order. As shown in Fig. 2, the average of nodal forces and thus the force density waves point mainly in radial direction. The value of the force densities in radial direction is greater than its value in the tangential direction. The acoustic noise, which is emitted from the stator, is induced by the radial force densities. The tangential forces excite structures, which are attached to the rotor. The noise emitted from the attached structures, e.g., gear, can be suppressed through minimizing the torque ripple.

The next step is to determine the radial force density waves that have major contribution to the acoustic radiation. It can be determined through measurement of SPL or estimated through simulation. By measuring the SPL, the dominant temporal orders of the acoustic radiation can be determined. Due to the high sound radiation, the lowest spatial order of these temporal orders should be chosen for further study [16]. Without measurement results or coupled 2-D electromagnetic and 3-D structural dynamic simulations [17], the dominant excitation of the acoustic radiation can only be estimated. Generally, the pair of dominant torque harmonics and the dominant force density waves with low temporal and spatial order should be analyzed.

The chosen force density waves are convoluted to identify the flux density waves, which have major contribution to these force densities. Depending on the result, the rotor and stator geometry or its winding can be altered to minimize the flux density harmonics in the air gap. This paper focuses on the flux density originated from the rotor and the alteration is performed on the outer surface of the rotor.

III. Alteration of Rotor's Surface

In this section, two approaches to reduce flux density harmonics by alternating the outer surface of the rotor will be introduced. The first approach is using the sinusoidal rotor field poles calculated with inverse cosine formula. The second approach is the notching of rotor's surface in d- or q-axis. The method to evaluate the influence of rotor's alteration on the air-gap flux density is described at the end of this section.

A. Sinusoidal Rotor Field Poles

Through methods introduced in [4], the harmonics of air-gap flux densities can be reduced and sinusoidal rotor field can be reached. The alteration of the rotor's surface is defined with the following equations:

$$\delta(\beta) = \frac{\delta_d}{\cos\left(\frac{\pi}{\tau_p}\beta\right)} \tag{8}$$

$$r_{\mathrm{rotor},o}(\beta) = r_{\mathrm{rotor},o} + \delta_d - \delta(\beta), \tag{9}$$

where δ_d is the air-gap length in the d-axis, τ_p is the pole pitch, β is the angle relative to d-axis of the rotor, and $\delta(\beta)$ and $r_{\mathrm{rotor},o}(\beta)$ are the air-gap length and rotor outer radius dependent on β, respectively. In Fig. 3, a half of a rotor pole is shown and the parameters in (8) and (9) are illustrated. According to the previous equations, the rotor outside the radius should follow the dashed contour pointed by $r_{\mathrm{rotor},o}(\beta)$. This parameter is limited with the rotor minimal outside radius $r_{\mathrm{rotor},o,\min}$ and hence the air-gap length in the q-axis δ_q. The ratio of the air-gap length in q- and d-axes ${}^{\delta_q}/_{\delta_d}$ is varied through augmenting the air gap in q-axis δ_q and its influence on the flux density composition is evaluated.

B. Notching of Rotor's Surface

As an alternative to Section III-A, the modifications of rotor surface on the d- and q-axes are considered. The cogging torque

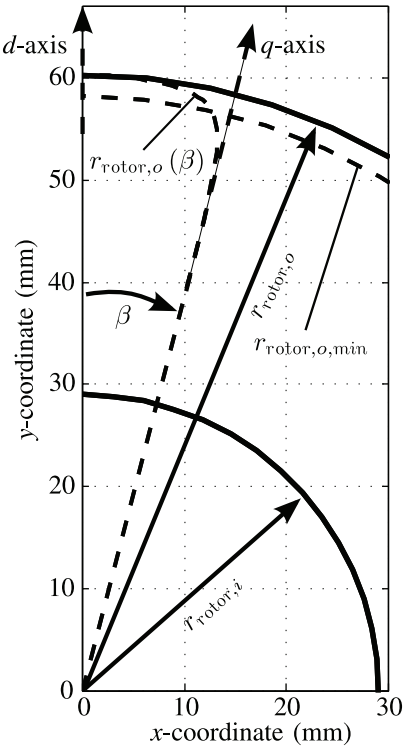

Fig. 3. Illustration of sinusoidal field pole and its parameters.

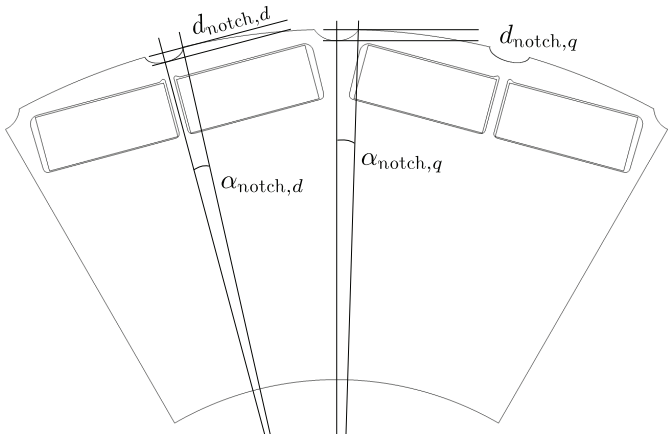

Fig. 4. Notch on d- and q-axes.

of an IPMSM can be reduced by notching the rotor surface in the d-axis [6] or q-axis [7]. The notch parameters are shown in Fig. 4, which are notch angle to d- or q-axes $\alpha_{\mathrm{notch},d/q}$ and notch depth $d_{\mathrm{notch},d/q}$. The origin of the axes are the center of the rotor. The influence of both parameters on the flux density harmonics is evaluated separately.

C. Evaluation of Flux Density Waves

The flux density harmonics originated from rotor are evaluated. The stator is treated as an ideal slotless stator, which is implemented in the FE simulation by applying Neumann boundary condition on the stator inner radius. With this method, there is only one time step required for the analysis of the flux density, since in this case, the flux density is not time dependent. The flux density in the middle of the air gap $r_{\delta,\mathrm{mid}} = 60.65\,\mathrm{mm}$ is sampled and Fourier transformed (spatial). The total harmonic distortion (THD) is evaluated with the following equation:

$$\mathrm{THD} = \sqrt{\frac{\sum\limits_{\mu>1} {B_{\mathrm{rad}}^{\mu}}^2}{\sum\limits_{\mu} {B_{\mathrm{rad}}^{\mu}}^2}}. \tag{10}$$

The objective of the rotor's surface alteration is to reduce the spatial flux density harmonics without reducing the fundamental wave significantly. In addition, the lower harmonics of the flux density have a major effect on the parasitic effects. Thus, the reduction in lower harmonics has a higher priority than reduction in the higher harmonics. Therefore, the evaluation criteria of the flux density harmonics are as follows:

1) the THD;
2) the value of the flux density's fundamental wave;
3) the value of the flux density's harmonics $\mu = 3, 5, 7$.

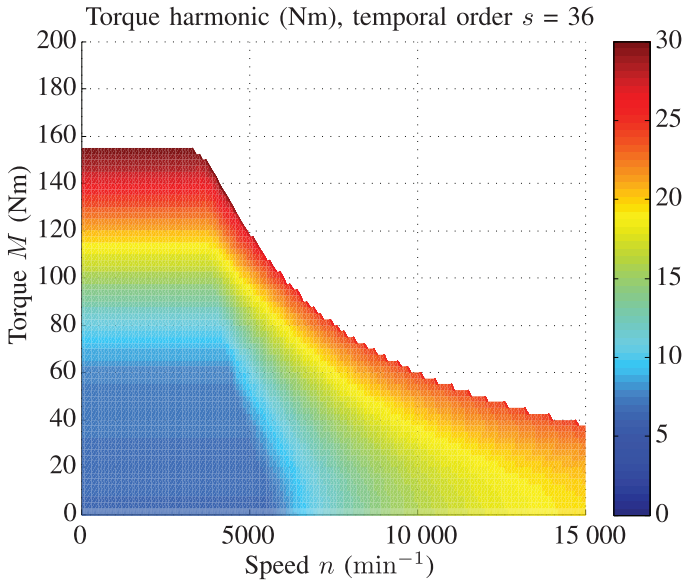

Fig. 5. Characteristic torque–speed diagram of the 36th harmonic of torque.

IV. Application on the IPMSM

The methods, which are explained in the previous sections, are applied to the examined IPMSM. First of all, the relevant operating points for the analysis have to be chosen. To examine the forces acting on the rotor, the torque harmonics have to be analyzed. The first dominant torque harmonic of the examined IPMSM is the 36th harmonic, which is the first slot harmonics. In Fig. 5, the characteristic torque–speed diagram of this harmonic is shown. From the diagram it could be concluded that the maximum of this harmonic is located at the maximum torque in the base speed area. The amplitude is 30 Nm, which represents 20 % of the average torque. The operating point between base speed and field-weakening area ($n = 3300\,\mathrm{min}^{-1}$ and $M = 155\,\mathrm{Nm}$) at the rated operating point is chosen for further examination.

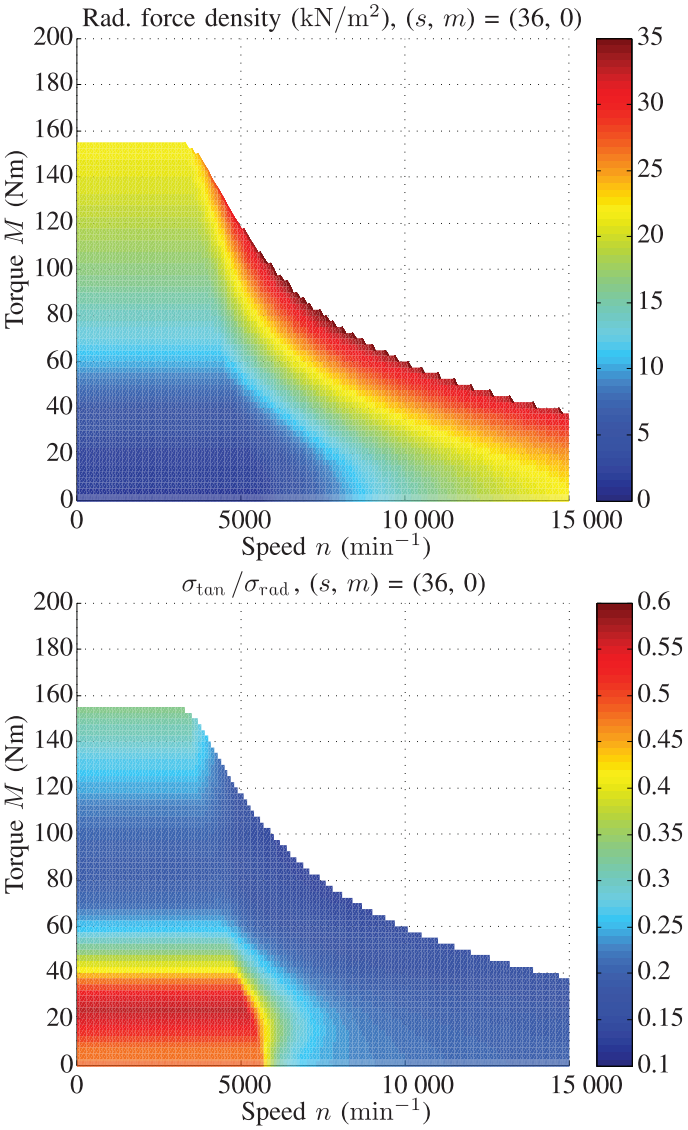

Fig. 6. Characteristic torque–speed diagram of the force density wave order (temporal s, spatial m) = (36, 0).

To examine the radial forces, which cause the deformation of the housing, the radial force density waves have to be analyzed. The low spatial orders m with highest value of the force densities have to be chosen. Only the positive temporal orders are taken into account, because the negative orders only contain redundant information [18]. According to [11], the dominant force density orders of the examined machine are (temporal s, spatial m): (12, 12), (24, −12), and (36, 0). The negative sign on the spatial order means reverse rotation relative to rotation direction of the rotor. In Fig. 6, the characteristic torque–speed diagram for the radial force density order (36, 0) and the ratio of tangential and radial force density of the same order are shown. It is shown that the tangential force density amplitudes are only 10 %–60 % of the radial force density amplitudes. To analyze the noise emission due to stator vibration, it is sufficient to examine the radial force density. The operating points with the highest radial force density value are chosen for further examination. The chosen operating points for the three aforementioned force density orders are listed in Table II. Calculation

TABLE II
OPERATING POINTS FOR CALCULATION OF SURFACE VELOCITIES

Force density orders (s, m) (kN/m^2)	Speed n (min^{-1})	Torque M (Nm)	Current I_{eff} (A)	Control angle ψ (°)
$\sigma_{\mathrm{DFT2}}(12, 12) = 200$	3300	155	210	−30
$\sigma_{\mathrm{DFT2}}(24, -12) = 22.2$	8000	30	95	−70
$\sigma_{\mathrm{DFT2}}(36, 0) = 36$	7400	82.5	200	−70

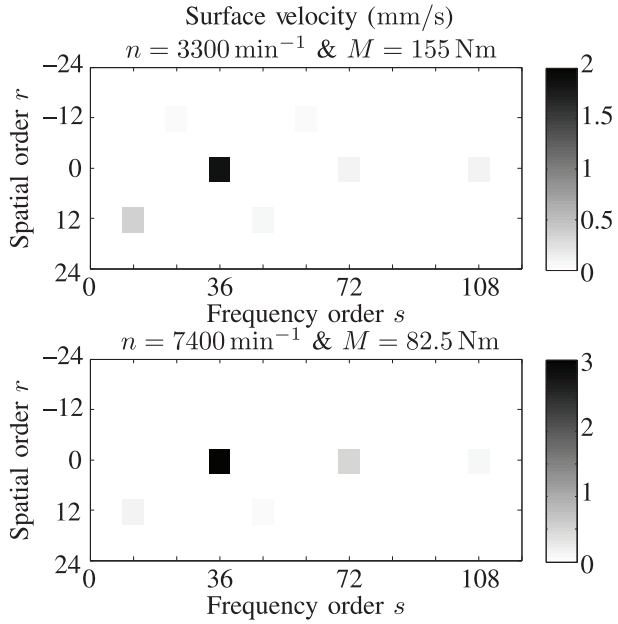

Fig. 7. Excited surface velocities at two operating points.

of surface velocities will be performed on these operating points.

In Fig. 7, the calculated surface velocities on the stator surface are shown. In all the studied operating points, the surface velocity reaches its maximum at temporal order $s = 36$ and spatial order $m = 0$. The next dominant orders are (s, m) = (72, 0) and (s, m) = (12, 12). It is shown that the values of the force densities are not directly correlated with the surface velocities, and therefore the acoustic radiation. The acoustic radiation is strongly dependent on the temporal and spatial orders of the force excitations. The frequencies of the noise excited from the force density order $(s, m) = (36, 0)$ between the speed $n = 3300{-}8000\,\mathrm{min}^{-1}$ lie between $f = 1980$ and $4800\,\mathrm{Hz}$. These frequencies are located in the area of the human sensitive hearing range. To improve the acoustic behavior of the IPMSM, this force density order has to be reduced. The operating point $n = 7400\,\mathrm{min}^{-1}$ and $M = 82.5\,\mathrm{Nm}$ shows the highest surface velocity order (36, 0), when compared to the other operating points. This radial force density order in the correspondent operating point will be convoluted to determine the contributing flux densities.

In Fig. 8, the decomposition of the radial force density order (36, 0) ($\sigma_{\mathrm{DFT2}}(36, 0)$) into its constructing force densities (numbered arrows) is shown. The vectors are sorted in descending order after their absolute value. The pairs of the flux density orders, which build each force density vectors, are listed in Table III. The flux densities originated from rotor can be

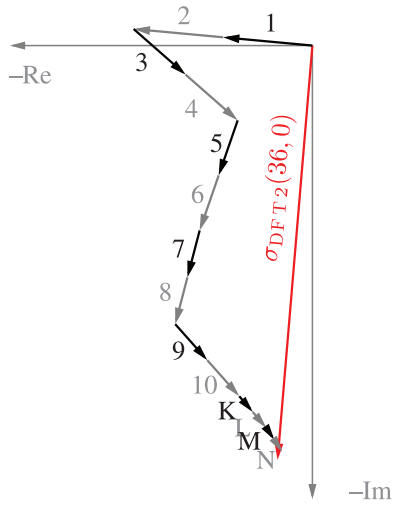

Fig. 8. Space-vector convolution of the force density order (36,0) at operating point $n = 7400\,\mathrm{min}^{-1}$ and $M = 82.5\,\mathrm{Nm}$.

TABLE III
CONTRIBUTING FLUX DENSITY ORDERS

Vector number	Flux density pair $B_{DFT2}(s,\nu/\mu)$	$B_{DFT2}(s,\nu/\mu)$
1 and 2	6, 6	30, –6
3 and 4	42, 42	6, –42
5 and 6	6, –6	42, 6
7 and 8	30, 30	6, –30
9 and 10	18, 18	18, –18
K and L	18, –18	54, 18
M and N	54, 54	18, –54

identified through the similar temporal and spatial orders: (6, 6), (18, 18), (30, 30), (42, 42), and (54, 54). The normed orders (after pole pair p and simulation of a time step) are first, third, fifth, seventh, and ninth, respectively. The fundamental wave is the order (6, 6) or the first order. The value of the higher harmonics has to be reduced, to improve the acoustic behavior. The objective is to alter the rotor flux density of the IPMSM into a sinusoidal form, as shown in Fig. 9. In the following sections, the rotor alteration will be performed and its effect on the flux density will be examined.

A. Sinusoidal Rotor Field Poles

Simulations of rotors with varied air-gap ratio $\delta_q/\delta_d = 1{-}3$ with an increment of 0.25 are performed. The minimum width of the bridge between the magnet and rotor outside contour is set to 0.3 mm. To meet this condition, the position of the magnets relative to rotor outside contour will be changed and their geometry are kept constant. The results are shown in Table IV. It is shown that the THD of the air-gap flux density decreases significantly until the air-gap ratio $\delta_q/\delta_d = 2$ is reached. The harmonics sink remarkably until the air-gap ratio $\delta_q/\delta_d = 1.75$. The fundamental wave of the flux density increases and reaches its maximum between $\delta_q/\delta_d = 2{-}2.75$. In Fig. 9, the spatial distribution of the flux densities for $\delta_q/\delta_d = 2$ and 2.25 are shown. They are compared to the flux density of the original IPMSM and a sine function. It is shown in the distribution that

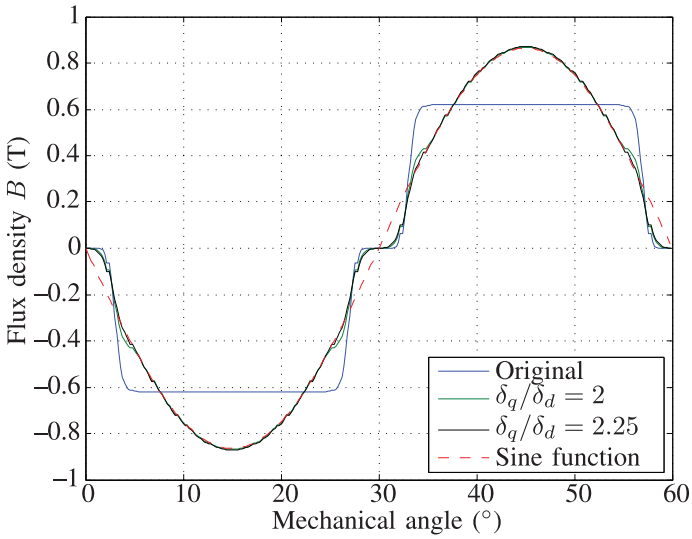

Fig. 9. Air-gap flux density of IPMSM rotor with and without sinusoidal field poles.

TABLE IV
VARIATION IN AIR-GAP RATIO δ_q/δ_d

Air gap ratio δ_q/δ_d	THD (%)	Flux density order (T) 1	3	5	7	9
1 (original)	24.38	0.75	0.15	0.01	0.06	0.07
1.25	17.73	0.77	0.09	0.02	0.05	0.07
1.5	11.81	0.80	0.04	0.01	0.03	0.06
1.75	8.54	0.84	0.01	0	0.03	0.04
2	6.91	0.86	0.01	0.02	0.03	0.03
2.25	6.42	0.86	0.02	0.02	0.03	0.03
2.5	6.23	0.86	0.02	0.03	0.03	0.02
2.75	5.98	0.86	0.02	0.03	0.03	0.02
3	5.53	0.85	0.02	0.02	0.02	0.02

the flux densities sampled at $\pm 10°$ from d-axis follow the sine function thoroughly. The difference between the two sinusoidal poles are insignificant. Due to the wider range of the similarity to the sine function, the rotor with air-gap ratio $\delta_q/\delta_d = 2.25$ is chosen for further examination.

B. Notching of Rotor's Surface

The variation in the notch parameters (angle α_{notch} and depth d_{notch}) in d- and q-axis are performed. The minimum width of the bridges is kept at 0.3 mm and the magnets' position is not changed. In Fig.10, the spatial distribution of the flux densities with notch in d- or q-axis is shown. The notch in d-axis causes a drop of the flux density in the position of the notch. The notch in q-axis induces a smoother transition of the flux density between the poles. The simulation results are listed in Tables V and VI. It is shown that the notch in the d-axis induces a lower fundamental wave of flux densities when compared to a rotor with a notch in q-axis. In both cases, the THD of the flux densities are higher than the original model. The notch in d-axis induces in general higher THD than notch in q-axis. The value of the seventh harmonic order can be lowered with both notch's position. The ninth harmonic order is additionally lowered in case of a notch in q-axis. The gray rows mark the geometry with

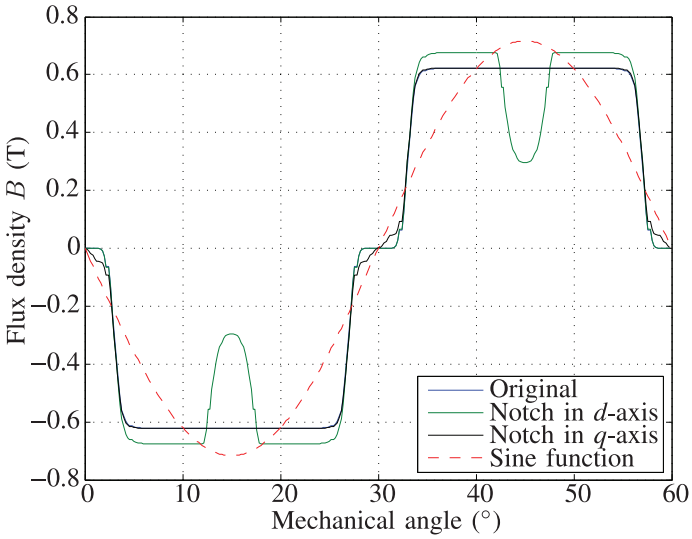

Fig. 10. Air-gap flux density of IPMSM rotor with and without notch in d- or q-axes.

TABLE V
VARIATION IN NOTCH PARAMETERS α_{notch} AND d_{notch} IN d-AXIS

Angle	Depth	THD	Flux density order (T)				
α_{notch} (°)	d_{notch} (mm)	(%)	1	3	5	7	9
0.9	0.25	26.63	0.74	0.16	0.02	0.05	0.09
0.9	2	29.47	0.74	0.18	0.04	0.04	0.10
0.5	0.5	25.73	0.75	0.15	0.01	0.06	0.07
2	0.5	32.48	0.73	0.2	0.06	0.02	0.1
1.5	0.5	30.11	0.74	0.19	0.04	0.03	0.01
2.5	1	38.22	0.72	0.25	0.09	0.01	0.12
4	1.5	49.44	0.68	0.34	0.13	0.03	0.08
5	1.75	55.64	0.66	0.39	0.13	0.08	0.04

TABLE VI
VARIATION IN NOTCH PARAMETERS α_{notch} AND d_{notch} IN q-AXIS

Angle	Depth	THD	Flux density order (T)				
α_{notch} (°)	d_{notch} (mm)	(%)	1	3	5	7	9
0.9	0.5	23.38	0.75	0.15	0.01	0.06	0.07
0.9	4	23.73	0.76	0.17	0.02	0.03	0.04
0.5	2.5	24.25	0.75	0.15	0	0.06	0.07
1	2.5	28.84	0.81	0.2	0.08	0.01	0.02
0.5	1.5	24.37	0.75	0.15	0.01	0.06	0.07
1	2.5	23.90	0.75	0.15	0	0.05	0.06
1.5	4	26.67	0.79	0.20	0.07	0.01	0.01
2	3.5	29.78	0.81	0.23	0.09	0.03	0

highest reduction the seventh harmonic order, which has vast contribution to the flux density order (36, 0) at $n = 7400\,\text{min}^{-1}$ and $M = 82.5\,\text{Nm}$ (Table III). These geometries are chosen for further examination.

C. Combination of Presented Approaches

As shown in Figs. 9 and 10, the combination of sinusoidal field poles and notches in q-axis show the most promising results. Through the sinusoidal field pole, the flux density near d-axis follow the shape of a sine function. The notch in q-axis leads to a smoother transition between the poles. The chosen air-gap ratio $\delta_q/\delta_d = 2.25$ ($\delta_q = 1.58\,\text{mm}$ and $\delta_d = 0.7\,\text{mm}$) and notch angle $\alpha_{\text{notch}} = 2°$ are implemented on the rotor. The chosen angle corresponds to the half of the pole transition angle in the flux density distribution. The depth of the notch d_{notch} is 3.5 mm, which is the maximum depth subjected to the condition of minimum width of the bridges. In this case, the value of the fundamental wave is 0.89 T, the THD is 1.69 %, and the value of the rest of the harmonics are under 0.005 T.

TABLE VII
SIMULATION RESULTS $I_{\text{eff}} = 200\,\text{A}$ AND $\psi = -70°$

Rotor alteration	$\sigma_{\text{DFT2}}(36,0)$ (kN/m^2)	$\dot{Y}(36,0)$ (mm/s)	M_{mean} (Nm)	$\frac{M_{\text{harm}}}{M_{\text{mean}}}$ (%) 36	72
Original	36	3.1	83.4	30.0	4.9
Sinusoidal field pole (SFP)	20	1.7	76.3	25.2	1.3
Notch in d-axis	34	2.9	78.2	39.1	5.8
Notch in q-axis	17	1.5	66.0	11.0	4.0
Combination SFP and q-notch	14	1.2	70.4	13.3	1.3

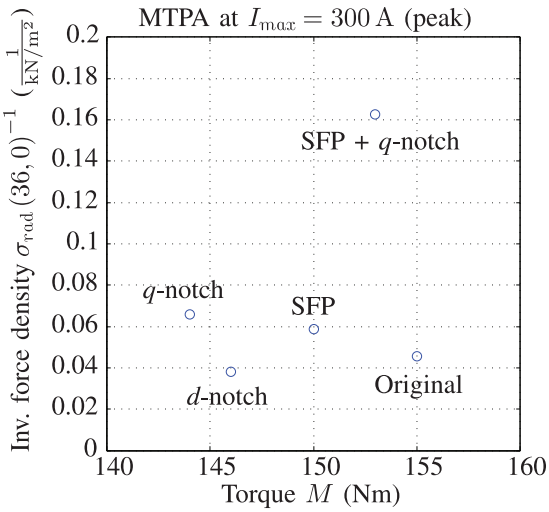

Fig. 11. Inverse of force density $\sigma_{\text{rad}}(36,0)^{-1}$ to torque at max. current I_{max} and optimal control angle ψ_{opt} (MTPA).

V. RESULTS

A. Analysis of an Operating Point

Simulations for the operating point with significant surface velocities ($I_{\text{eff}} = 200\,\text{A}$ and $\psi = -70°$) for the chosen geometries are performed. The results are listed in Table VII. It is shown that sinusoidal field pole and notch in q-axis are effective to reduce the radial force density $\sigma_{\text{DFT2}}(36,0)$ and the related surface velocity $\dot{Y}(36,0)$. Thus, the acoustic emission is likely to be reduced. Due to change of the reluctance, the effective torque of these variants is reduced, particularly of the rotor with notch in q-axis. However, the torque harmonics are also decreased. The notch in d-axis does not have considerable advantage to torque and noise production. The combination of sinusoidal field pole and notch in q-axis shows the best noise emission and proportion of mean torque and its harmonics.

In Fig. 11, a scatter plot of the torque and the inverse of radial force density order (36, 0) at maximal current with optimal control angle (MTPA) of the chosen rotor geometries is shown. The

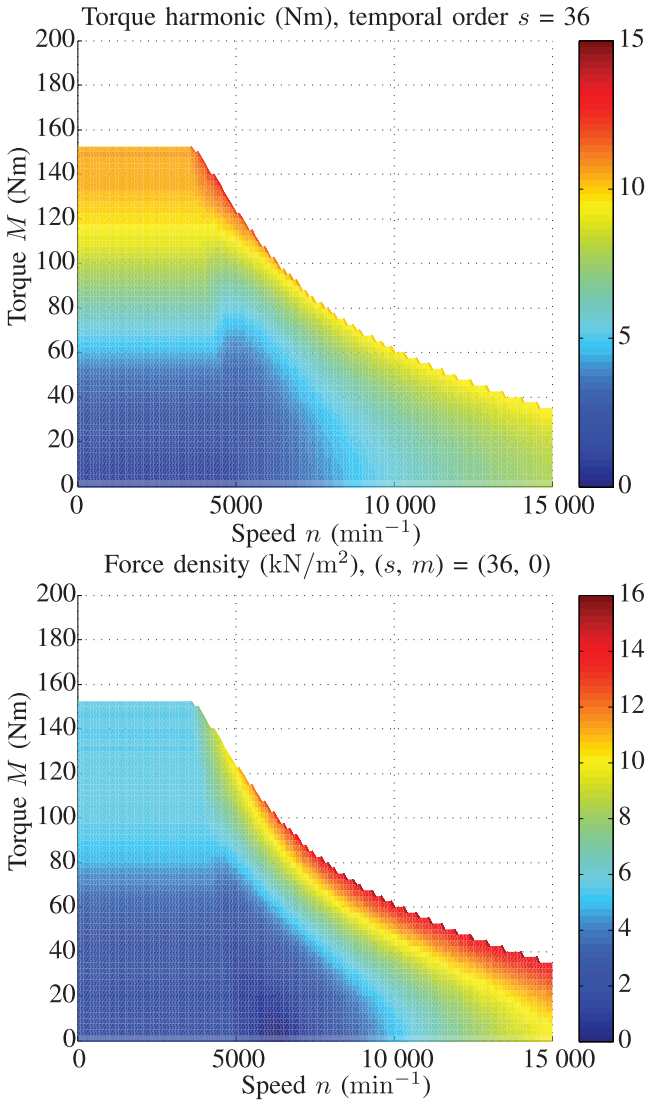

Fig. 12. Characteristic torque–speed diagram of the (top) 36th torque harmonic and the (bottom) force density order (temporal s, spatial m) = (36, 0).

objective of the taken measures is to minimize the force excitation. To simplify the analysis, the inverse values of the force density are utilized. It is shown that the combination of sinusoidal field pole and notch in q-axis shows the lowest force density with acceptable mean torque. When compared to the original geometry, the mean torque sinks only by 1.3 % but the radial force density by 72 %. To study the effect of the taken measures, this geometry will be examined for the entire operating area defined with MTPA and MTPV control.

B. Analysis of the Entire Operating Area

As mentioned in Section V-A, the reluctance behavior of the machine is modified due to alteration of the rotor's surface. Hence, the currents' and controls' angle after MTPA and MTPV control of the operating points (torques and speeds) are also shifted. In Fig. 12, the characteristic torque–speed diagram of the 36th torque harmonic and the radial force density wave order (36, 0) are shown. Due to the change of

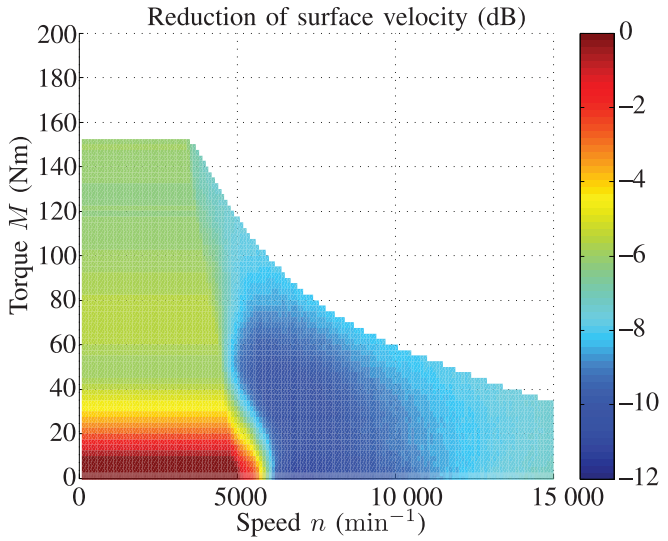

Fig. 13. Characteristic torque–speed diagram of the surface velocity reduction, calculation based on the dominant harmonics.

reluctance, the maximum torque of the IPMSM is reduced by 2.5 Nm. The 36th torque harmonic at its shifted rated speed $n = 3600\,\mathrm{min}^{-1}$ is 11.27 Nm, which represents 7.4 % of the mean torque. The maximum value of the radial force density order (36, 0) is 15 kN/m^2 at $n = 9600\,\mathrm{min}^{-1}$ and $M = 65\,\mathrm{Nm}$. In Fig. 13, the reduction in the surface velocity due to the taken measures is shown. The lower harmonics orders: (12, 12), (24, -12), (36, 0), (48, 12), (60, -12), and (72, 0) are taken into account for the calculations. It is shown that the surface velocities are reduced for the whole operating points.

VI. Conclusion

It has been shown that using the proposed method, the noise, vibration, and harshness (NVH) behavior of the IPMSM can be improved. Through alteration of the rotor surface, the harmonics of the air-gap flux density can be reduced. This correlates with the distribution of the force densities acting on the stator teeth, which are responsible for the noise emission. The noise reduction is obtained by the reduction in the relevant force density order and thus the related surface velocities. The combination of sinusoidal field pole and notch in q-axis shows the most promising results. In this case, the relevant torque harmonic 36th and radial flux density order (36, 0) are reduced at least by 58 %. The surface velocity are reduced up to 12 dB.

References

[1] S. A. Gelfand, *Essentials of Audiology*. New York, NY, USA: Thieme Med. Publishers, 2009.
[2] D. Franck, M. van der Giet, and K. Hameyer, "Towards low audible noise drives for FEV applications," in *Proc. 14th Int. Power Electron. Motion Control Conf. (EPE/PEMC)*, 2010, pp. S11-25–S11-30.
[3] H. Jordan, *Geräuscharme Elektromotoren*. Essen, Germany: W. Girardet, 1950.
[4] R. Richter, *Elektrische Maschinen: Allgemeine Berechnungselemente*. Basel, Switzerland: Birkhäuser, 1951.
[5] S. E. Abdollahi and S. Vaez-ZAdeh, "Reducing cogging torque in flux switching motors with segmented rotor," *IEEE Trans. Magn.*, vol. 49, no. 10, pp. 5304–5309, Oct. 2013.

[6] S. Huang, J. Liu, J. Gao, and L. Xiao, "Optimal design of the rotor structure for interior permanent magnet synchronous motor," in *Proc. Int. Conf. Power Eng. Energy Elect. Drives (PowerEng)*, 2011, pp. 1–5.
[7] K.-W. Jeon, T.-Y. Lee, Y.-J. Kim, and S.-Y. Jung, "Numerical shape design characteristics of torque ripple reduction for interior permanent magnet synchronous motor," in *Proc. 9th IET Int. Conf. Comput. Electromagn. (CEM)*, 2014, pp. 1–2.
[8] R. De Doncker, D. Pulle, and A. Veltmann, *Advanced Electrical Drives: Analysis, Modeling Control*. New York, NY, USA: Springer, 2010.
[9] S. Rick, A. K. Putri, D. Franck, and K. Hameyer, "Hybrid acoustic model of electric vehicles: Force excitation in permanent magnet synchronous machine," in *Proc. IEEE Int. Elect. Mach. Drives Conf. (IEMDC)*, 2015, pp. 1419–1425.
[10] G. Müller, K. Vogt, and B. Ponick, *Berechnung elektrischer Maschine*. Hoboken, NJ, USA: Wiley, 2008.
[11] J. Gieras, C. Wang, and J. C. Lai, *Noise of Polyphase Electric Motor*. Boca Raton, FL, USA: CRC Press, 2006.
[12] Z. Q. Zhu and D. Howe, "Improved methods for prediction of electromagnetic noise radiated by electrical machines," *Proc. Inst. Elect. Eng.—Elect. Power Appl.*, vol. 141, no. 2, pp. 109–120, Mar. 1994.
[13] M. van der Giet, R. Rothe, M. H. Gracia, and K. Hameyer, "Analysis of noise exciting magnetic force waves by means of numerical simulation and a space vector definition," in *Proc. 18th Int. Conf. Elect. Mach. (ICEM)*, 2008, pp. 1–6.
[14] F. Henrotte, M. Felden, M. van der Giet, and K. Hameyer, "Electromagnetic force computation with the eggshell method," in *Proc. 14th Int. Symp. Numer. Field Calcul. Elect. Eng. (IGTE)*, 2010.
[15] F. Henrotte, G. Deliege, and K. Hameyer, "The eggshell approach for the computation of electromagnetic forces in 2D and 3D," *COMPEL, Int. J. Comput. Math. Elect. Electron. Eng.*, vol. 23, no. 4, pp. 996–1005, 2004.
[16] T. E. McDevitt, R. L. Campbell, and D. M. Jenkins, "An investigation of induction motor zeroth-order magnetic stresses, vibration, and sound radiation," *IEEE Trans. Magn.*, vol. 40, no. 2, pp. 774–777, Mar. 2004.
[17] M. van der Giet, C. Schlensok, B. Schmülling, and K. Hameyer, "Comparison of 2-D and 3-D coupled electromagnetic and structure-dynamic simulation of electrical machines," *IEEE Trans. Magn.*, vol. 44, no. 6, pp. 1594–1597, Jun. 2008.
[18] J. S. Lim, *Two-Dimensional Signal and Image Processing*. Englewood Cliffs, NJ, USA: Prentice-Hall, 1990.

Aryanti Kusuma Putri received the M.Sc. degree in electrical engineering from RWTH Aachen University, Aachen, Germany, in 2013.

She has been a Research Associate with the Institute of Electrical Machines, RWTH Aachen University, since June 2013. Her research interests include contactless power transmission, parasitic effects in electrical machines, and simulation and design of electrical machines.

Sebastian Rick received the Dipl.-Ing. degree in electrical engineering from RWTH Aachen University, Aachen, Germany, in 2012.

He has been a Research Associate with the Institute of Electrical Machines, RWTH Aachen University, since June 2012. His research interests include new arts of electrical machines and simulation and acoustical design of electrical machines.

David Franck received the Dipl.-Ing. degree in electrical engineering from RWTH Aachen University, Aachen, Germany, in 2008.

He was a Staff (Research Associate) with the Institute of Electrical Machines, RWTH Aachen University, where, since 2011, he has been a Chief Engineer. His research interests include acoustic behavior of electrical machines.

Kay Hameyer (M'96–SM'99) received the M.Sc. degree in electrical engineering from the University of Hanover, Hanover, Germany, in 1986, and the Ph.D. degree for work on permanent-magnet excited machines from the University of Technology Berlin, Berlin, Germany, in 1992.

After his university studies, he worked with Robert Bosch GmbH, Stuttgart, Germany, as a Design Engineer for permanent-magnet servo motors. From 1988 to 1993, he was a member of staff with the University of Technology Berlin. From 1996 to 2004, he was a Full Professor of Numerical Field Computations and Electrical Machines, Katholieke Universiteit Leuven (KU Leuven), Leuven, Belgium. Since 2004, he has been a Full Professor and the Director of the Institute of Electrical Machines (IEM), RWTH Aachen University, Aachen, Germany. His research interest focuses on all aspects of the design, control, and manufacturing of electrical machines and the associated numerical simulation. The characterization and modeling of hard- and soft-magnetic materials is another focus of his work. His research interests include numerical field computation and optimization, the design and control of electrical machines, in particular, permanent-magnet excited machines and induction machines. He has authored/coauthored more than 250 journal publications, more than 500 international conference publications, and four books

Dr. Hameyer has been a member of the German VDE since 2004 and a Fellow of the Institution of Engineering and Technology, U.K., since 2002.